| | | | | | |
|---|---|---|---|---|---|
| Iwata, A., Nagata, K., Hatsuta, H., Takuma H., Bundo, M., Iwamoto, K., Tamaoka, A., Murayama, S., Saido, T., Tsuji, S. | Altered CpG methylation in sporadic Alzheimer's disease is associated with APP and MAPT dysregulation. | **Hum. Mol. Genet.** | 23 | 648-656 | 2013 |
| Maruyama, M., Shimada, H., Suhara, T., Shinotoh, H., Ji, B., Maeda, J., Zhang, M.R., Trojanowski, J.Q., Lee, V.M., Ono, M., Masamoto, K., Takano, H., Sahara, N., Iwata, N., Okamura, N., Furumoto, S., Kudo, Y., Chang, Q., Saido, T.C., Takashima, A., Lewis, J., Jang, M.K., Aoki, I., Ito, H., Higuchi, M. | Imaging of tau pathology in a tauopathy mouse model and in Alzheimer patients compared to normal controls. | **Neuron** | 79 | 1094-1108 | 2013 |
| Hosokawa M, Arai T, Yamashita M, Tsuji H, Nonaka T, Masuda-Suzukake M, Tamaoka A, Hasegawa M, Akiyama H. | Differential diagnosis of amyotrophic lateral sclerosis from Guillain-Barré syndrome by quantitative determination of TDP-43 in cerebrospinal fluid. | **Int J Neurosci.** | | | in press |
| Hasegawa M, Watanabe S, Kondo H, Akiyama H, Mann DM, Saito Y, Murayama S | 3R and 4R tau isoforms in paired helical filaments in Alzheimer's disease. | **Acta Neuropathol.** | 127 | 303-5 | 2014 |

| | | | | | |
|---|---|---|---|---|---|
| Mann DM, Rollinson S, Robinson A, Bennion Callister J, Thompson JC, Snowden JS, Gendron T, Petrucelli L, Masuda-Suzukake M, Hasegawa M, Davidson Y, Pickering-Brown S. | Dipeptide repeat proteins are present in the p62 positive inclusions in patients with frontotemporal lobar degeneration and motor neurone disease associated with expansions in *C9ORF72*. | **Acta Neuropathol Commun.** | 1 | 68 | 2013 |
| Dan A, Takahashi M, Masuda-Suzukake M, Kametani F, Nonaka T, Kondo H, Akiyama H, Arai T, Mann DM, Saito Y, Hatsuta H, Murayama S, Hasegawa M. | Extensive deamidation at asparagine residue 279 accounts for weak immunoreactivity of tau with RD4 antibody in Alzheimer's disease brain. | **Acta Neuropathol Commun.** | 1 | 54 | 2013 |
| Nonaka T, Masuda-Suzukake M, Arai T, Hasegawa Y, Akatsu H, Obi T, Yoshida M, Murayama S, Mann DM, Akiyama H, Hasegawa M. | Prion-like properties of pathological TDP-43 aggregates from diseased brains. | **Cell Rep.** | 4 | 124-34 | 2013 |
| Moujalled D, James JL, Parker SJ, Lidgerwood GE, Duncan C, Meyerowitz J, Nonaka T, Hasegawa M, Kanninen KM, Grubman A, Liddell JR, Crouch PJ, White AR. | Kinase Inhibitor Screening Identifies Cyclin-Dependent Kinases and Glycogen Synthase Kinase 3 as Potential Modulators of TDP-43 Cytosolic Accumulation during Cell Stress. | **PLoS One.** | 8 | e67433 | 2013 |

| | | | | | |
|---|---|---|---|---|---|
| Masuda-Suzukake M, Nonaka T, Hosokawa M, Oikawa T, Arai T, Akiyama H, Mann DM, Hasegawa M. | Prion-like spreading of pathological alpha-synuclein in brain. | **Brain.** | 136 | 1128-38 | 2013 |
| Kimura T, Tsutsumi K, Taoka M, Saito T, Masuda-Suzukake M, Ishiguro K, Plattner F, Uchida T, Isobe T, Hasegawa M, Hisanaga S. | Isomerase Pin1 Stimulates Dephosphorylation of Tau Protein at Cyclin-dependent Kinase (Cdk5)-dependent Alzheimer Phosphorylation Sites. | **J Biol Chem.** | 288 | 7968-77 | 2013 |
| | | | | | |
| | | | | | |
| | | | | | |

# IV.研究成果の刊行物・別刷

*The American Journal of Pathology, Vol. 180, No. 5, May 2012*

*DOI: 10.1016/j.ajpath.2012.01.015*

*Matrix Pathobiology*

# Heparan Sulfate Subdomains that are Degraded by Sulf Accumulate in Cerebral Amyloid ß Plaques of Alzheimer's Disease

## *Evidence from Mouse Models and Patients*

Tomomi Hosono-Fukao,* Shiori Ohtake-Niimi,*† Hitomi Hoshino,* Markus Britschgi,‡ Hiroyasu Akatsu,§ Md. Motarab Hossain,* Kazuchika Nishitsuji,¶ Toin H. van Kuppevelt,‖ Koji Kimata,** Makoto Michikawa,¶ Tony Wyss-Coray,‡ and Kenji Uchimura*†¶

*From the Section of Pathophysiology and Neurobiology,* Department of Alzheimer's Disease Research,¶ National Center for Geriatrics and Gerontology, Obu, Japan; the Department of Biochemistry,† Graduate School of Medicine, Nagoya University, Nagoya, Japan; the Department of Neurology and Neurological Sciences,‡ Stanford University School of Medicine, Stanford, California; the Choju Medical Institute,§ Fukushimura Hospital, Toyohashi, Japan; the Department of Biochemistry,‖ Radboud University Nijmegen Medical Center, Nijmegen, The Netherlands; and the Research Complex for the Medicine Frontiers,** Aichi Medical University, Nagakute, Japan*

**Alzheimer's disease (AD) is characterized by extracellular cerebral accumulation of amyloid β peptide (Aβ). Heparan sulfate (HS) is a glycosaminoglycan that is abundant in the extracellular space. The state of sulfation within the HS chain influences its ability to interact with a variety of proteins. Highly sulfated domains within HS are crucial for Aβ aggregation *in vitro*. Here, we investigated the expression of the sulfated domains and HS disaccharide composition in the brains of Tg2576, J20, and T41 transgenic AD mouse models, and patients with AD. RB4CD12, a phage display antibody, recognizes highly sulfated domains of HS. The RB4CD12 epitope is abundant in the basement membrane of brain vessels under physiological conditions. In the cortex and hippocampus of the mice and patients with AD, RB4CD12 strongly stained both diffuse and neuritic amyloid plaques. Interestingly, RB4CD12 also stained the intracellular granules of certain hippocampal neurons in AD brains. Disaccharide compositions in vessel-enriched and nonvasculature fractions of Tg2576 mice and AD patients were found to be comparable to those of non-transgenic and non-demented controls, respectively. The RB4CD12 epitope in amyloid plaques was substantially degraded *ex vivo* by Sulf-1 and Sulf-2, extracellular HS endosulfatases. These results indicate that formation of highly sulfated HS domains may be upregulated in conjunction with AD pathogenesis, and that these domains can be enzymatically remodeled in AD brains. *(Am J Pathol 2012, 180: 2056–2067; DOI: 10.1016/j.ajpath.2012.01.015)***

Heparan sulfate (HS) is a linear polysaccharide that exists in large quantities in the extracellular space. One or more HS chains are covalently bound to a core protein comprising heparan sulfate proteoglycan (HSPG).[1,2] HS chains and heparins, structural analogues of HS chains, are a family of glycosaminoglycans consisting of repeating disaccharide units of glucuronic/iduronic acid and glucosamine. Modification with sulfation as well as elongation of these disaccharides is enzymatic,[3] bestowing on the chains structural diversity.[4–6] HS contains highly

This work was supported by grants from the Japanese Health and Labour Sciences Research (Comprehensive Research on Aging and Health H19-001 and H22-007 to K.U., H20-007 to M.M.), Grants-in-Aid from the Ministry of Education, Science, Sports and Culture (22790303 to K.U. and JBBNNR, Comprehensive Brain Science Network to H.A.), and in part from the Sanofi-Aventis Science Foundation of Japan (to K.U.), the Naito Science Foundation (to K.U.), the Takeda Science Foundation (to K.U.), and the Daiko Foundation (to K.U.).

Accepted for publication January 19, 2012.

Present address of M.B., F. Hoffmann-La Roche Ltd, pRED, CNS Discovery, CH-4070, Basel, Switzerland.

Supplemental material for this article can be found on *http://ajp.amjpathol.org* or at doi: 10.1016/j.ajpath.2012.01.015.

Address reprint requests to Kenji Uchimura, Ph.D., Department of Biochemistry, Graduate School of Medicine, Nagoya University, 65 Tsurumai, Showa, Nagoya, Aichi, 466-8550 Japan. E-mail: arumihcu@med.nagoya-u.ac.jp.

sulfated domains and partially sulfated or non-sulfated domains, which are transitional.[3] Highly sulfated domains are formed by consecutive clusters of sulfated disaccharides. It has been shown that a trisulfated disaccharide structure [-iduronic acid(2S)-Glucosamine(NS,6S)-] occurs within highly sulfated domains. RB4CD12, a phage display anti-HS antibody, has been shown to recognize trisulfated disaccharide-containing HS subdomains[7–9] Trisulfated disaccharides are considered to be key elements in molecular interactions between HS/heparin and many ligands, including growth factors and morphogens.[1,10] Trisulfated disaccharides, as well as the RB4CD12 epitope, are degraded by extracellular sulfatases, Sulf-1, and Sulf-2.[8,11,12] In the brain, we have shown that the RB4CD12 HS domains are abundantly present in the vasculature[9] and that these domains can be degraded by the Sulfs *ex vivo*.[8] However, the roles of the RB4CD12 HS domains in pathological and physiological processes in brain vasculature are not known.

Alzheimer's disease (AD) is a progressive neurodegenerative disorder. One of the pathological hallmarks of AD is the presence of extracellular amyloid plaques in brain areas that are responsible for cognition and memory functions. The predominant composition of amyloid plaques is fibrils made of amyloid $\beta$ peptide (A$\beta$). A great deal of biochemical and genetic evidence has indicated that aggregation and accumulation of A$\beta$ in toxic forms within the extracellular space play a central role in AD pathogenesis. One of the authors previously reported that certain structures of HS chains exist in amyloid plaques of AD brains,[13] and that structural variation of HSPG correlates with amyloid plaque formation in the brains of AD patients.[14] HSPG is also known to facilitate cerebral amyloid deposition induced exogenously in a rat model *in vivo*.[15] Functional roles of HS and HSPG in AD pathology are proposed to be acceleration of A$\beta$ fibril formation and protection of the fibril against microglial phagocytosis.[16] It was reported that the aggregation state of A$\beta$ requires its binding properties to heparin.[17] Pathological correlations between the RB4CD12 HS domains, which are rich in heparin and AD have not been established. Here we present evidence that the RB4CD12 HS domains are accumulated in cerebral amyloid plaques of transgenic AD mouse models and patients with AD, and that these HS epitopes can be degraded by Sulf-1 and Sulf-2 *ex vivo*.

## Materials and Methods

### Materials

The RB4CD12 phage display-derived anti-heparan sulfate antibody was produced in a vesicular stomatitis virus (VSV)-tag version and purified as previously described.[7] Alternative nomenclature of RB4CD12 is HS3A8. The following materials were commercially obtained from the sources indicated. Heparinases (I, II and III), polyclonal rabbit anti-laminin antibody (Ab), horseradish peroxidase-conjugated monoclonal anti-VSV Ab, and Cy3-conjugated monoclonal anti-VSV Ab were from Sigma (St. Louis, MO); biotinylated monoclonal anti-amyloid $\beta$ (N-terminus) Ab (82E1) was from IBL (Gunma, Japan); polyclonal rabbit anti-VSV Ab was from Bethyl Laboratories (Montgomery, TX); Cy2-conjugated goat anti-mouse IgG (H+L), Cy2-conjugated goat anti-rabbit IgG (H+L), Cy2-conjugated goat anti-rat IgG (H+L) Abs, and Cy2-conjugated streptavidin were from Jackson ImmunoResearch Laboratories (West Grove, PA); rabbit anti-Iba1 Ab was from Wako Pure Chemical Industries, Ltd. (Osaka, Japan); rabbit anti-glial fibrillary acidic protein and monoclonal anti-phospho-PHF-tau pThr231 (AT180) Abs were from Thermo Scientific (Rockford, IL); goat anti-mouse syndecan-3 Ab was from R&D Systems, Inc (Minneapolis, MN); rabbit anti-glypican-1 (M-95) Ab was from Santa Cruz Biotechnology, Inc (Santa Cruz, CA); polyclonal goat anti-rabbit IgG Nanogold, $\phi$1.4 nm, was from Nanoprobes (Yaphank, NY); and horseradish peroxidase-conjugated goat anti-rabbit IgG was from Cell Signaling Technology, Inc. (Beverly, MA).

### Animals

C57BL/6 mice were from Japan SLC Inc. (Hamamatsu, Japan). Heterozygotic transgenic mice that expressed the human amyloid precursor protein bearing the Swedish (K670N, M671L) mutation (Tg2576 strain),[18] the Swedish and Indiana (V717F) mutations (J20 strain),[19] or the Swedish and London (V717I) mutations (T41 strain)[20] were maintained in barrier facilities. Tg2576 mice were purchased from Taconic Farms, Inc., Hudson, NY. J20 mice were from the Jackson Laboratory (Bar Harbor, ME). The National Center of Geriatrics and Gerontology Institutional Animal Care and Use Committee approved the animal studies.

### Human Postmortem Brain Tissues

Patients with sporadic AD received a pathological diagnosis according to the criteria of the Consortium to Establish a Registry for Alzheimer's Disease and the Braak stage. Non-demented controls were elderly patients who were age-matched and without significant neurological disorders. Patients were also cognitively evaluated by neuropsychological tests using the Mini-Mental State Examination and Hasegawa's dementia scale, which is commonly used in Japan. Entorhinal cortex and hippocampus postmortem tissue samples from neurologically unimpaired subjects (non-demented controls [NDCs]) and from subjects with AD were obtained under Committees on Human Research approval of National Center for Geriatrics and Gerontology and Choju Medical Institute of Fukushimura Hospital. Diagnosis of AD was confirmed by pathological and clinical criteria (Table 1). The incidence of vascular risk factors (eg, atherosclerosis, myocardial infarction, and so forth), the sex ratio, age, and the postmortem interval were comparable between NDC and AD (Table 1). Tissue was cut and frozen or fixed with formalin, and then embedded with paraffin. Frozen tissues were subjected to structural analysis of HS. The embedded tissues were cut using a microtome.

**Table 1.** Clinical and Neuropathological Characteristics of Alzheimer's Disease and Non-Demented Control Donor Patients used in the Disaccharide Composition Analysis of Heparan Sulfate

| Patient number | Age (years) | Sex | Stage of amyloid deposits (0, A, B, C)* | NFT stage (I–VI) | Cerebral amyloid angiopathy | Vascular risk factors | PMI (hr) |
|---|---|---|---|---|---|---|---|
| Alzheimer's disease patients | | | | | | | |
| 0508 | 94 | F | C | V | + | CI | 43 |
| 0512 | 83 | F | C | VI | + | ATH | 2 |
| 0604 | 91 | F | C | V | – | CI | 8 |
| 0805 | 93 | F | C | VI | + | CI | 27 |
| 0810 | 80 | M | C | V | – | CI | 15 |
| 0811 | 81 | M | C | VI | – | – | 8 |
| 0814 | 91 | M | C | V | + | – | 5 |
| 0824 | 87 | F | B | VI | – | – | 9 |
| Age-matched non-demented controls | | | | | | | |
| 0707 | 95 | F | A | II | – | MI | 4 |
| 0710 | 83 | F | A | II | – | CH/CI | 24 |
| 0601 | 90 | F | B | II | – | MI | 4 |
| 0802 | 93 | F | A | III | – | CH/CI | 20 |
| 0704 | 84 | M | B | II | – | CI | 3 |
| 0807 | 82 | M | 0 | I | – | CH | 8 |
| 0908 | 91 | M | A | II | – | – | NA |
| 0903 | 87 | F | 0 | II | – | CI | 7 |

*0 = none, A = rare or a few, B = mild or moderate, C = numerous or marked.
ATH, atherosclerosis; CH, cerebral hemorrhage; CI, cerebral infarction; F, female; M, male; MI, myocardial infarction; NA, not applicable; NFT, neurofibrillary tangle; PMI, postmortem interval.

## *Fractionation of Brain Samples*

A snap-frozen mouse cortex (~25 mg) was placed in a tube containing 600 μL (30 volume of the tissue weight) of ice-cold Tris-buffered saline (TBS) (20 mmol/L Tris and 137 mmol/L NaCl, pH 7.6) and protease inhibitors (complete protease inhibitor cocktail; Roche Diagnostics, Mannheim, Germany). The tube was placed in a water bath of the Bioruptor ultrasonic vibration (CosmoBio, Tokyo). The tissue was fragmented by sonicating the tube for 15 seconds with the maximum ultrasonic wave output power 4 to 5 times until solid materials in the tube became invisible. The material was ultracentrifuged at 100,000 × *g* for 20 minutes at 4°C. The supernatant was collected and stored frozen as TBS or "TBS soluble fraction." The resulting precipitate was suspended in 600 μL (the same volume as previously described) of TBS containing 1% SDS. The suspension was centrifuged at 12,000 rpm for 20 minutes at room temperature. The resulting supernatant was collected and stored frozen as TBS or "TBS-insoluble/1% SDS-soluble fraction." The protein concentrations of both fractions were measured with a BCA Protein Assay Reagent Kit (Thermo Scientific). Brain cortices were dissected out from 3 Non-Tg or 3 Tg2576 18-month-old mice and then snap frozen. Brain samples were put together, placed on a glass Petri dish, and minced with a blade. The tissues were transferred into a tube containing 1 mL of ice-cold TBS. The tissues were homogenized with a Dounce homogenizer. The homogenate was filtered with a 100-μm nylon mesh. The filtered materials on the mesh were collected and then subjected to the structural analysis described as follows ("vessel-enriched fractions"). Materials filtered through the 100-μm nylon mesh were collected and then analyzed ("non-vasculature fractions"). Methylene blue staining and bright field microscopy confirmed cerebral blood vessels on the filters.

## *Immunohistochemistry*

Fresh mouse brains were embedded in O.C.T. compound (Sakura Finetek, Torrance, CA) and frozen in liquid nitrogen. The brains were stored at −80°C until analysis. Cryostat-cut sections (10-μm thick) were prepared on MAS-coated glass slides (Matsunami, Osaka, Japan), fixed in ice-cold acetone for 15 minutes, and then air-dried for 30 minutes. Sections were incubated with blocking solution (3% bovine serum albumin in PBS) for 15 minutes at RT. Sections were washed twice with PBS and then incubated with a mixture of RB4CD12 (1:100 dilution), rabbit anti-laminin antibody (1:100 dilution, Sigma), and biotinylated 82E1 (1:50 dilution) overnight at 4°C. Then, primary antibodies were detected with Cy3-conjugated monoclonal anti-VSV-G (4 μg/mL), Cy2-conjugated polyclonal goat anti-rabbit IgG (3 μg/mL), and aminomethylcoumarin acetate-conjugated streptavidin (6.8 μg/mL, Jackson ImmunoResearch, West Grove, PA). Sections were mounted in FluorSave Reagent (Merck, Darmstadt, Germany). Digital images were captured by fluorescent microscopy (model BX50, Olympus, Tokyo, Japan) at the same setting for each antibody. The fluorescently stained area was quantitatively determined using Image-Pro Plus software (Media Cybernetics, Bethesda, MD). To determine the effects of the Sulfs and heparinases, 3% bovine serum albumin-blocked sections were pre-treated with 100 μL of a reaction mixture containing 5 μmol HEPES, pH 7.5, 1 μmol $MgCl_2$, and enzymes at 37°C overnight. Recombinant human Sulf-1 (0.4 μg) and human Sulf-2 (0.4 μg) were prepared from conditioned medium of transfected HEK293 cells and used as previously described.[8] For pretreatment with heparitinases, a mixture of 1 mU heparinase I, 0.25 mU heparinase II, and 0.1 mU heparinase III were added to the

reaction mixture. Cy2-conjugated streptavidin was used to detect bound 82E1. Human brain sections (4-$\mu$m thickness) were obtained from paraffin-embedded tissue blocks. After deparaffinization and rehydration, endogenous peroxidase activity was quenched with 3% $H_2O_2$ (Sigma). Sections were subjected to heat-induced epitope retrieval followed by IgG blocking using M.O.M. kit (Vector Laboratories Inc., Burlingame, CA). Sections were incubated with RB4CD12 (1:100 dilution) overnight at 4°C. Bound antibody was detected with horseradish peroxidase-conjugated mouse anti-VSV followed by visualization with diaminobenzidine (3,3′-diaminobenzidinetetrahydrochloride) supplied with the EnVision reagent (Dako Japan, Tokyo, Japan).

### *Immunoelectron Microscopy*

Cryostat-cut sections from 17-month-old Tg2576 mouse brains were prepared on MAS-coated glass slides, fixed in 4% paraformaldehyde for 5 minutes, and then washed with PBS for 1 hour. Sections were incubated with 3% bovine serum albumin for 30 minutes at RT. Diluted RB4CD12 antibody (1:40) was then applied overnight. After washing, diluted rabbit anti-VSV secondary antibody (7.2 $\mu$g/mL) was applied for 1 hour. After several washes, diluted goat anti-rabbit IgG antibody coupled with 1.4-nm-diameter tertiary gold particles (1:40) was applied for 30 minutes. The samples were then washed and fixed in 2% glutaraldehyde in 0.1 M sodium cacodylate buffer (pH 7.4) for 3 hours, followed by enlargement of the gold particles with an HQ-Silver Enhancement Kit (Nanoprobes). The specimens were examined in a Hitachi H-7600 transmission electron microscope (Hitachi Koki, Tokyo, Japan).

### *Immunoblots*

The proteins (40 $\mu$g per lane) were separated by NuPAGE 3% to 8% polyacrylamide gel electrophoresis (Invitrogen, Carlsbad, CA), and blotted onto a polyvinylidene difluoride membrane (Millipore, Billerica, MA). The membrane was blocked with 5% skim milk/PBS 0.1% Tween for 1 hour at room temperature and then incubated overnight with RB4CD12 antibody (1:500) in TBS 0.1% Tween at 4°C. The membrane was washed and incubated with horseradish peroxidase-conjugated mouse anti-VSV (1:2000) for 1 hour at RT. Bound antibodies were visualized with SuperSignal West Dura Chemiluminescent reagent (Thermo Scientific). Signals were visualized and quantified using a LAS-3000 mini luminescent image analyzer (Fujifilm, Tokyo, Japan).

### *Preparation and Structural Analysis of HS*

There were 100 mg of frozen brain tissues or the cortical vessel residue that remained on filters previously described, which was suspended in 2 mL of 0.2N NaOH and incubated overnight at RT. The samples were neutralized with 4 N HCl and then treated with DNase I and RNase A (0.04 mg/mL each) (Roche Diagnostics) in 50 mmol/L Tris-HCl, pH8.0, 10 mmol/L $MgCl_2$ for 3 hours at 37°C. Subsequently, the samples were treated with actinase E (0.08 mg/mL) (Kaken Pharmaceutical Co., Ltd., Tokyo, Japan) overnight at 37°C. The supernatant was collected by centrifugation at 5000 × *g* at 4°C for 10 minutes after heat inactivation of the enzyme and then mixed with the same volume of 50 mmol/L Tris-HCl, pH 7.2. The HS was purified by DEAE-Sepharose column chromatography.[9] The disaccharide compositions of the HS were determined by reversed-phase ion-pair chromatography with postcolumn fluorescent labeling.

### *Quantitative Real Time-PCR for Expression of Genes Related to HS Synthesis*

Total RNA was extracted from frozen mouse cortices using TRIZol Reagent (Invitrogen). Total RNA (4 $\mu$g was used for reverse transcription reaction in 100 $\mu$L of buffer with random hexamers, using Superscript II Reverse Transcriptase (Invitrogen). PCR was conducted in duplicate with 20-$\mu$L reaction volumes of SYBR Premix Ex TaqII (Takara Bio Inc. Shiga, Japan), 0.2 $\mu$mol/L of each primer and 2 $\mu$L of the cDNA reaction mixture. PCR was performed using the following parameters: 95°C, 10 seconds, 1 cycle; 95°C, 5 seconds; and 60°C, 30 seconds, 40 cycles. Analysis was performed using sequence detection software supplied with Thermal Cycler Dice Real Time System TP800 (Takara Bio Inc.). mRNA levels of each gene were normalized by comparison to $\beta$-actin mRNA levels. Conclusions are drawn from duplicate PCR reactions at least two independent reverse transcription reactions. Primer sequences used in this study are as indicated for *Ndst1*, 5′-GCAGATGGCCCTGAACAAGAA-3′ and 5′-GCACGTGCACAGGGTACACA-3′; for N-deacetylase/*N*-sulfotransferase 2 (*Ndst2*), 5′-TCATCCAGAAGTTCCTGGGTATCAC-3′ and 5′-AGACAGCGAGTCTTACCACCTTCAA-3′; for *Ndst3*, 5′-TCTGGTGTCAGCTGCTGGAAG-3′ and 5′-CACGTTGTGGTCGCGGTAGTAG-3′; for *Ndst4*, 5′-TTGTTCCCAAAGCCAAGATCATTAC-3′ and 5′-TCAGGGCAGCTGGATCTTCA-3′; for *Hs6st1*, 5′-CTGACTGGACCGAACTCACCAA-3′ and 5′-TCTCGCAGCAGGGTGATGTAGTAG-3′; for *Hs6st2*, 5′-AAACTTCAACTCAGGCGCCAAC-3′ and 5′-CTCCATTCACTCAAGTACCGTGACA-3′; for *Hs6st3*, 5′-GACTGGACCGAGCTCACCAA-3′ and 5′-CATGCTTCCATTCGCTCAGGTA-3′; for *Hs2st1*, 5′-GCAAGCACCTCGTTCACCAA-3′ and 5′-CATCTCGTTCCAGGTGGTTATGTTC-3′; for *Sulf1*, 5′-CCACATGGAGTTCACCAACGTC-3′ and 5′-TAGCCGTGGTCCGCAGTGTA-3′; for *Sulf2*, 5′-GAGTACCAGACAGCATGCGAACA-3′ and 5′-TTGGGCACCAGGTTGGAGA-3′; and for *Actb*, 5′-CATCCGTAAAGACCTCTATGCCAAC-3′ and 5′-ATGGAGCCACCGATCCACA-3′.

### *Statistical Analysis*

All data are presented as means ± SD unless noted otherwise. The values were analyzed by unpaired Student's *t*-test using Prism software (GraphPad Software, La Jolla, CA). *P* values less than 0.05 were considered to be statistically significant.

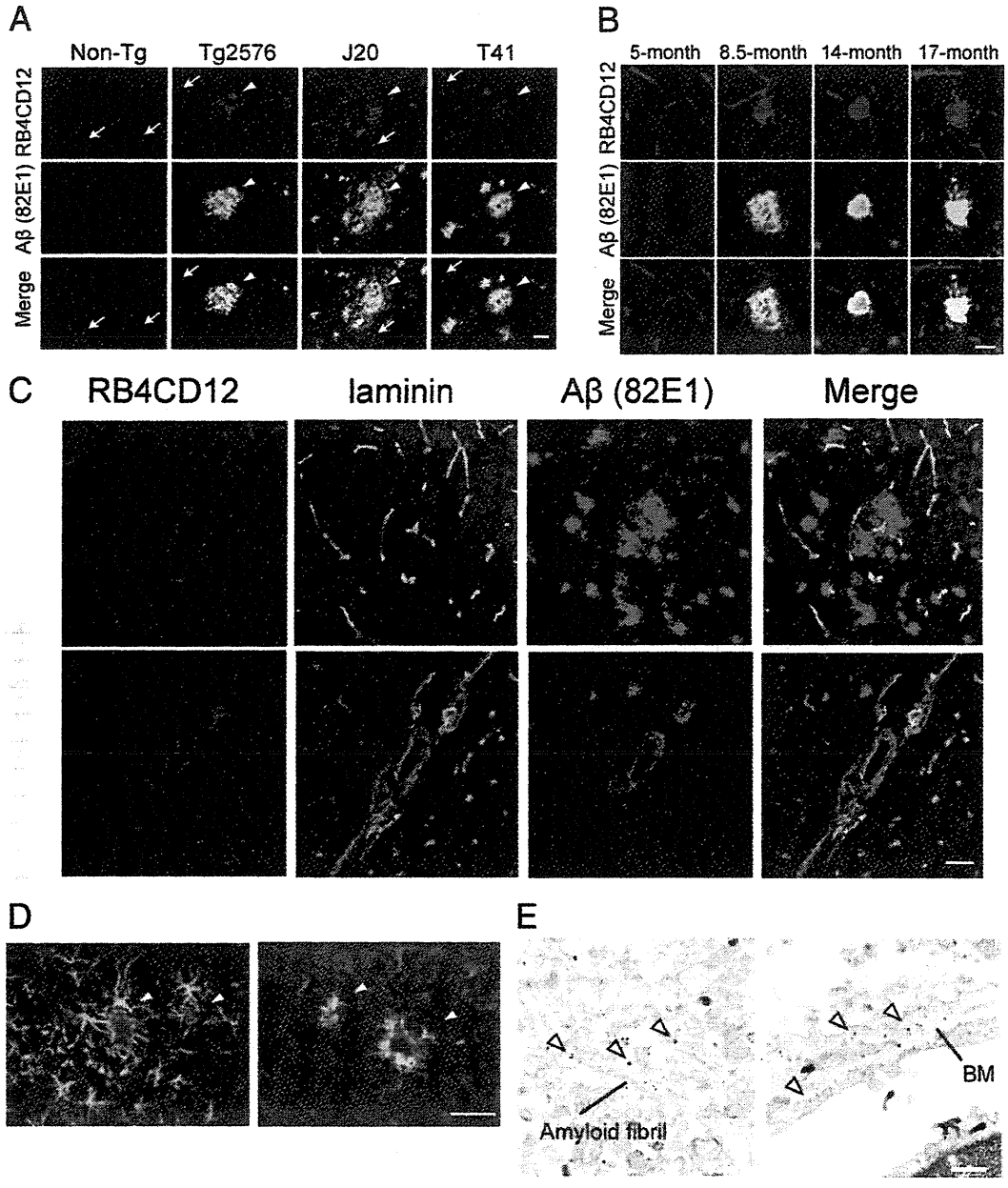


**Figure 1.** RB4CD12 anti-heparan sulfate epitope colocalizes with amyloid β plaques in the brain of Tg2576, J20, and T41 mice. **A:** Cryostat-cut brain sections of 18-month-old non-Tg and Tg2576, 23-month-old J20, and 12-month-old T41 mice were stained with RB4CD12 anti-HS antibody (red) and 82E1 anti-amyloid β (Aβ) antibody (green). Staining signals in vessels (**arrows**) and amyloid plaques (**arrowheads**) are shown. **B:** Expression of the RB4CD12 epitope and Aβ in aging Tg2576 brain. **C:** Expression of the RB4CD12 epitope, Aβ and laminin, a marker for vessels in the 18-month-old Tg2576 brain. **D:** Co-staining of RB4CD12 anti-HS antibody (red) with cell type-specific antibodies against glial fibrillary acidic protein astrocytes (**left**) or Iba1 microglia (**right**) (green). Co-stained areas are shown in yellow. **E:** Immunoelectron microscopy for the RB4CD12 epitope in amyloid fibrils in the brain of 18-month-old Tg2576 mouse. **Left panel** shows RB4CD12 signals in amyloid fibrils indicated by **arrowheads**. **Right panel** shows RB4CD12 signals in the basement membrane of vessels. BM, basement membrane. Scale bars (in **A**, **C**, and **D**): 50 μm. Scale bars (in **B** and **E**): 20 μm and 500 nm, respectively.

## *Results*

### *Immunoreactivity of RB4CD12 Anti-Heparan Sulfate is Colocalized with Aβ Plaques in Brains of Transgenic Mouse Models of AD*

RB4CD12 scFv antibody recognizes trisulfated disaccharide-containing highly sulfated domains within HS.[8,21] The RB4CD12 epitope has been shown to be present abundantly in the vasculature of the brain in mice.[9] We first analyzed expression of the RB4CD12 epitope in the brain of transgenic mouse models of AD. Tg2576 mice express mutated human amyloid precursor protein in the brain and show numerous Aβ plaques in the cortex and hippocampus.[18] The localization of the RB4CD12 highly sulfated domains in Aβ plaques was observed in an 18-month-old Tg2576 hippocampus (Figure 1A). The RB4CD12 epitope was immunolocalized in both diffuse

and neuritic amyloid plaques in the brain of Tg2576 (Figure 1, A–C). RB4CD12 also detected brain microvessels in Tg2576 mice. No specific staining was observed when RB4CD12 was substituted with MPB49, a non-HS scFv antibody (not shown). We also tested aged J20 and T41, other mouse models of AD. With respect to expression levels of Aβ peptides, Aβ42 is dominant in J20 and T41 mouse brains, whereas Aβ40 is dominant in Tg2576 mouse. We examined brain sections of these model mice immunohistochemically. The RB4CD12 highly sulfated domains were colocalized with Aβ plaques in the hippocampus of 23-month-old J20 and 12-month-old T41 mice (Figure 1A). To analyze age-dependent accumulation of the RB4CD12 epitope in Aβ plaques, we collected Tg2576 brains from 5-, 8.5-, 14- and 17-month-old mice. Aβ plaques were observed in 8.5-, 14- and 17-month-old Tg2576 brains. Cerebral Aβ deposition increases with age. RB4CD12 stained Aβ plaques at these ages (Figure 1B). Next, we investigated vasculature and non-vasculature RB4CD12 epitopes in aged Tg2576 brain by co-staining with antibodies against Aβ and laminin, a marker of vascular basement membranes. Immunoreactivity of RB4CD12 in vascular structure was colocalized with anti-laminin staining signals (Figure 1C). RB4CD12 staining signals that were not associated with signals of anti-laminin antibody predominantly colocalized with anti-Aβ staining signals in the cortex of Tg2576 mice (Figure 1C, upper panels). The RB4CD12 epitope was also observed in the vessel walls of Aβ-positive leptomeningeal vessels (Figure 1C, lower panels). Staining patterns of RB4CD12 were different from the immunoreactivity of glial fibrillary acidic protein, an astrocyte marker, and Iba-1, a microglia marker (Figure 1D). Immunoelectron microscopy confirmed the localization of RB4CD12 epitope within amyloid fibrils and the basement membrane (Figure 1E). The RB4CD12 immunoreactive area that is not colocalized with anti-laminin staining signals was determined by fluorescence microscopy and quantified with computer-aided image analysis. In Tg2576 cortex and hippocampus, RB4CD12-positive but laminin-negative area was increased to fourfold to fivefold of that in non-Tg (Figure 2). In contrast, no change was observed in the cerebellum where no Aβ plaques were observed (Figure 2). We noted that laminin-positive vessels had attenuated diameters and a more ragged profile in Tg2576 cortex and hippocampus (Figure 2).

## *The RB4CD12 Epitope Is Immunolocalized in Amyloid Plaques in Postmortem Brains of Alzheimer's Disease Patients*

We tested RB4CD12 antibody for staining of brains from NDC individuals and AD patients (Table 1). In NDCs, vessel-staining signals were predominantly observed (Figure 3A). In AD entorhinal cortex, amyloid deposits, as well as vessels, were positive for RB4CD12 (Figure 3B). Amyloid deposits and microvessels were also stained with RB4CD12 in AD hippocampus (Figure 3C). Interestingly, some pyramidal neurons in AD hippocampus showed intracellular granular staining (Figure 3D). These intracellular staining signals were detected in a certain number of cells that were positive for hyperphosphorylated microtubule-associated protein tau as revealed by the AT180 monoclonal antibody (see Supplemental Figure S1 at *http://ajp.amjpathol.org*).

## *Expression of the RB4CD12 Epitope Borne in Molecules with 70–180 kDa Molecular Weights Is Upregulated in the Cortex of Tg2576 Mice*

As an extension of the staining results in the mouse and human brain tissues, we wished to determine which proteins contain the RB4CD12 epitope and were differentially expressed in Tg2576 brains. We performed Western blotting for cortex samples, which were fractionated as TBS-insoluble/1% SDS-soluble. Four non-Tg and five Tg2576 mice (20 months old) were examined. Multiple bands were positive for RB4CD12 antibody in both non-Tg and Tg2576 (Figure 4A). We measured intensities of 460 kDa, 180 kDa, 120 kDa, and 100–70 kDa bands by densitometry. There was a 1.3-fold increase in the intensity of overall RB4CD12 recognition determinants in Tg2576 brain extracts compared with non-Tg controls (Figure 4B). Expression levels of RB4CD12 epitopes in bands of 180 kDa, 120 kDa, and 100–70 kDa were increased 1.1- to 1.5-fold in the cortex of Tg2576 mice (Figure 4B). There was no significant change in the intensity of bands of 460 kDa. Syndecan-3 and glypican-1 are HSPGs expressed in glial cells surrounding Aβ plaques of Tg2576 mice.[22] To ascertain whether these proteins are HSPGs that contain the RB4CD12 epitope, we then analyzed their expression. Western blotting revealed the protein bands at 250 to 180 kDa for syndecan-3 and 60 kDa for glypican-1 in the cortex of Tg2576 mice (see Supplemental Figure S2A at *http://ajp.amjpathol.org*). Expression levels of these proteins in the Tg2576 cortex were comparable to those in non-Tg controls (see Supplemental Figure S2B at *http://ajp.amjpathol.org*).

## *Disaccharide Compositions of HS and Expression Profiles of HS Enzymes in the Cortex of Tg2576 and Postmortem AD*

We performed structural analysis of HS chains extracted from mouse and human postmortem brains (Table 1). HS was isolated from the cortex of mice or postmortem human entorhinal cortex. HS was depolymerized into its constituent disaccharides by a mix of bacterial heparitinases. The disaccharide compositions of the HS were determined by reversed-phase ion-pair chromatography. We found that the total HS contents and HS disaccharide compositions in vessel-enriched fractions ("vessel-enriched fr") and non-vessel associated fractions ("non-vasculature fr") were comparable between non-Tg and Tg2576 mice (Figure 4C). In human, the reduction in the proportion of non-sulfated disaccharides reached statistical significance. Total HS contents and percentages of other sulfated disaccharides were comparable between NDC and AD (Figure 4D). To understand possible mechanisms of upregulation of the RB4CD12 epitope in AD mouse brains, we measured mRNA levels of 10 HS modification enzymes by quantitative real time-PCR. HS enzymes include sulfotransferases and extracellular sulfatases. These enzymes are regarded as

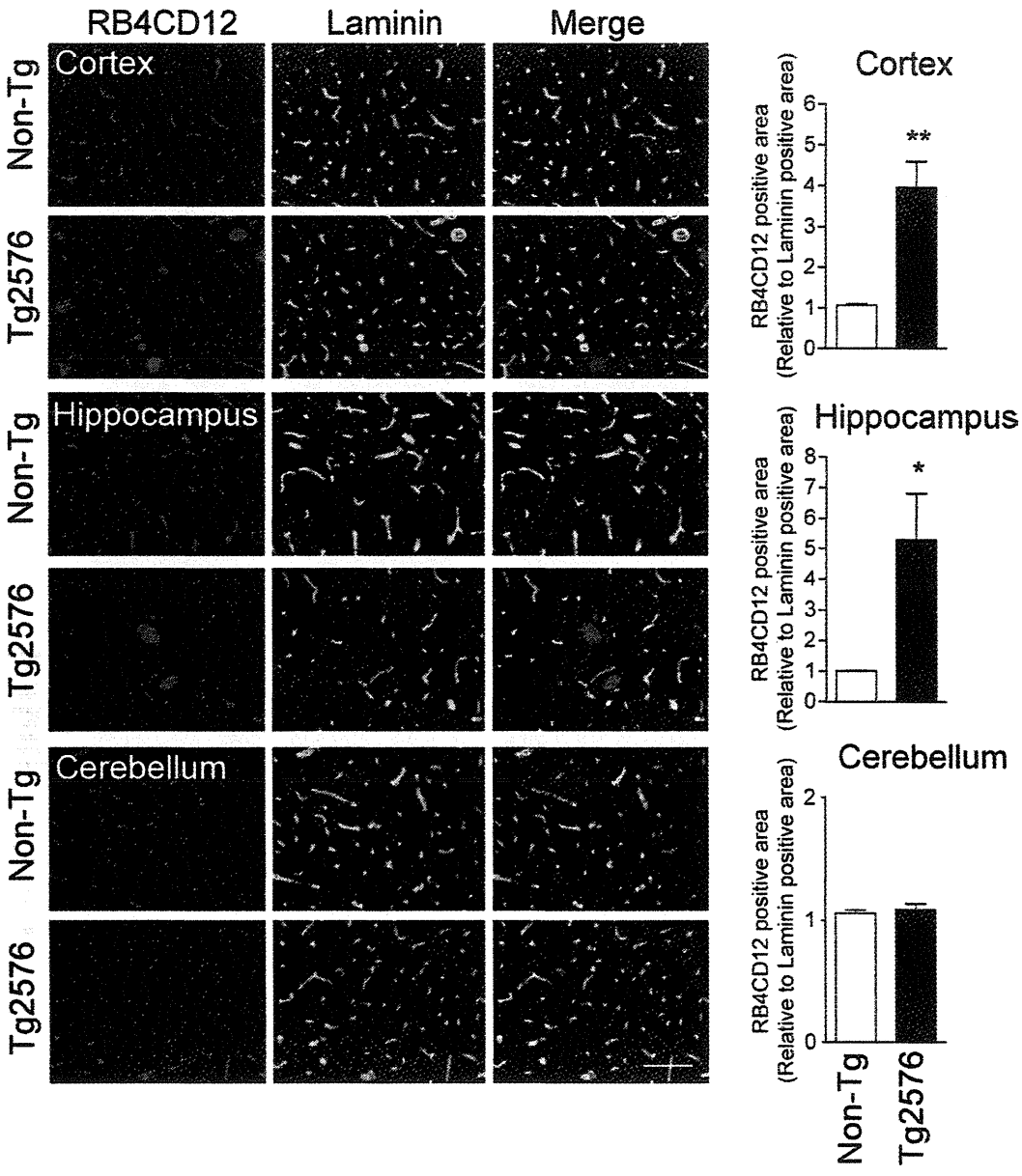


**Figure 2.** Quantification of the RB4CD12 epitope in nonvascular parenchyma in the brain of Tg2576 mice. Cryostat-cut brain sections of Tg2576 mice were stained with RB4CD12 (red) and anti-laminin (green) antibodies. Laminin is a marker for brain vessels. Nonvascular amyloid $\beta$ plaques were stained with RB4CD12 antibody in the cortex and hippocampus. Graphs are of semiquantitative analysis of immunohistochemical pictures of RB4CD12 and laminin. RB4CD12-positive areas that were not colocalized with anti-laminin staining signals were calculated. $^{*}P < 0.05$, $^{**}P < 0.01$.

key molecules in the regulation of sulfation of HS. The mRNA level of N-deacetylase/N-sulfotransferase 2 were significantly increased in Tg2576 (24%) (Figure 4E). The mRNA levels of Sulf-1 and Sulf-2 were comparable between non-Tg and Tg2576 mice (Figure 4E).

### *Sulf-1 and Sulf-2, Extracellular HS Sulfatases, Degrade the RB4CD12 Epitope Accumulated in Amyloid Plaques*

Previously, we showed that the treatment of wild-type mouse brain sections with Sulf-1 or Sulf-2 greatly diminished the RB4CD12 epitope abundant in vasculature.[8] To determine whether the RB4CD12 epitope in amyloid plaques is susceptible to Sulf-1 and Sulf-2 and degraded by these enzymes, we treated cryo-cut brain sections of 18-month-old Tg2576 mice with recombinant Sulf-1, Sulf-2, or conditioned medium of MCF-7 breast cancer cells, which secrete native Sulf-2.[23] These treatments substantially reduced the RB4CD12 epitope in sections of Tg2576 brain *ex vivo* (Figure 5). A mixture of bacterial heparinases confirmed that the assay is suitable for *ex vivo* degradation of HS in brain sections and that the observed signals arose from HS (Figure 5). Anti-A$\beta$ staining signals that were colocalized with the RB4CD12 epitope were retained after Sulf treatment (Figure 5).

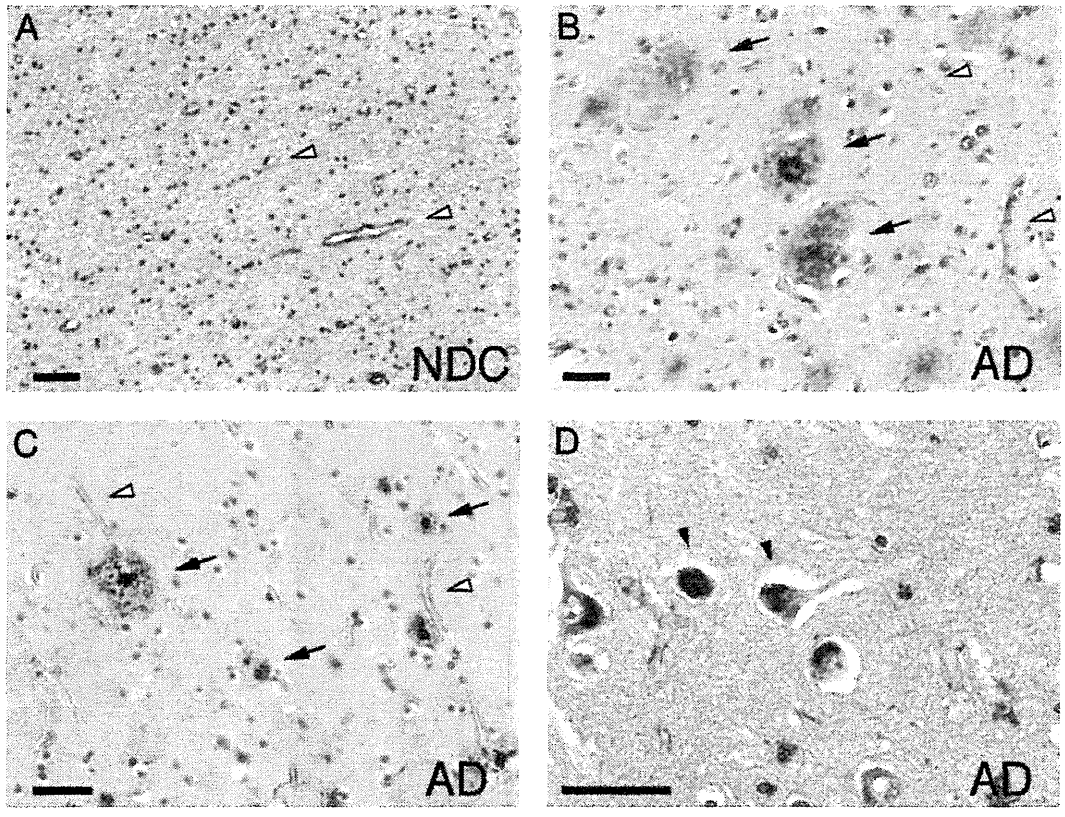


**Figure 3.** RB4CD12 epitope immunolocalizes in amyloid plaques in the brains of Alzheimer's disease patients. Immunoperoxidase staining for RB4CD12 (brown) in the entorhinal cortex (**A**, **B**) and hippocampus (**C**, **D**). **Open arrowheads** in **A**–**C** show vessel-staining signals in brains of non-demented control (NDC) and Alzheimer's disease (AD). In AD, amyloid deposits were also positive for RB4CD12 (**arrows** in **B** and **C**). Intracellular RB4CD12-staining signals are seen in some hippocampal neurons of AD (**arrowheads** in **D**). Scale bars: 50 μm.

## *Discussion*

In the present study, we showed that the RB4CD12 epitope is colocalized with amyloid plaques in brains of AD mouse models and patients with AD. Consistent with our previous report,[9] the RB4CD12 epitope was also colocalized with laminin-positive vasculature in brains of mouse models of AD. Quantification analysis revealed that the non-vascular RB4CD12-positive area was increased in the cortex and hippocampus of Tg2576, J20, and T41 AD models. In the cerebellum, where no amyloid plaques were observed in these model mice, RB4CD12 staining was comparable to that in the non-Tg. Morphological alterations of the vasculature observed in the cortex and hippocampus of Tg2576 were consistent with the previous report that Aβ aggregates induce the structural and functional disruption of smooth muscle cells in the vasculature.[24] Results in aging brains of Tg2576 mice suggested that Aβ and the HS highly sulfated domains start accumulation at the same age. Aβ and other self-aggregating peptides share cationic motifs that may be involved in binding to the negative charges of sulfated glycosaminoglycan.[25,26] HS and other glycosaminoglycan chains can stabilize mature fibrils against proteolytic degradation.[27] HS facilitates the formation of fibrils of amylin,[17] apo-serum amyloid A,[28] α-synuclein,[29] prion protein,[30] muscle acylphosphatase,[31] transthyretin,[32] Tau,[33] and Aβ.[34–36] *In vivo* fragmentation of heparan sulfate by heparanase overexpression could protect mice from amyloid protein A amyloidosis.[37] Importantly, the degree of sulfation is critical for enhancement of fibrillogenesis of Aβ.[35] Pathological effects of heparin in Aβ aggregation assays are dependent on sulfate moieties at N- and O-positions.[38] Our findings of selective accumulation of the RB4CD12 epitope in amyloid plaques suggest that highly sulfated domains of HS could play an important role in the progression of Aβ deposition. HSPG facilitates cerebral amyloid deposition, which can be induced exogenously in a rat model.[15] Highly sulfated HS chains could be one candidate for heat-resistant materials present in the brain extract that are essential for exogenous induction of cerebral β-amyloidogenesis in mouse models.[39] Recently, Timmer et al[40] demonstrated that only a minimal number of Aβ plaques (~30%) were co-stained with the epitope of JM403, an anti-HS antibody, in aging brains of APPswe/PS1dE9 model mice. JM403 detects HS subdomains containing the positively charged disaccharide [-glucuronic/iduronic acid-N-unsubstituted glucosamine].[41] Future studies may reveal differential contribution of HS subdomains composed of specific disaccharide structures to AD pathogenesis. Possible involvement of the RB4CD12 epitope existing in laminin-positive vasculature in AD pathogenesis should also be clarified in the future. Interestingly, intraneuronal RB4CD12 staining was observed in the

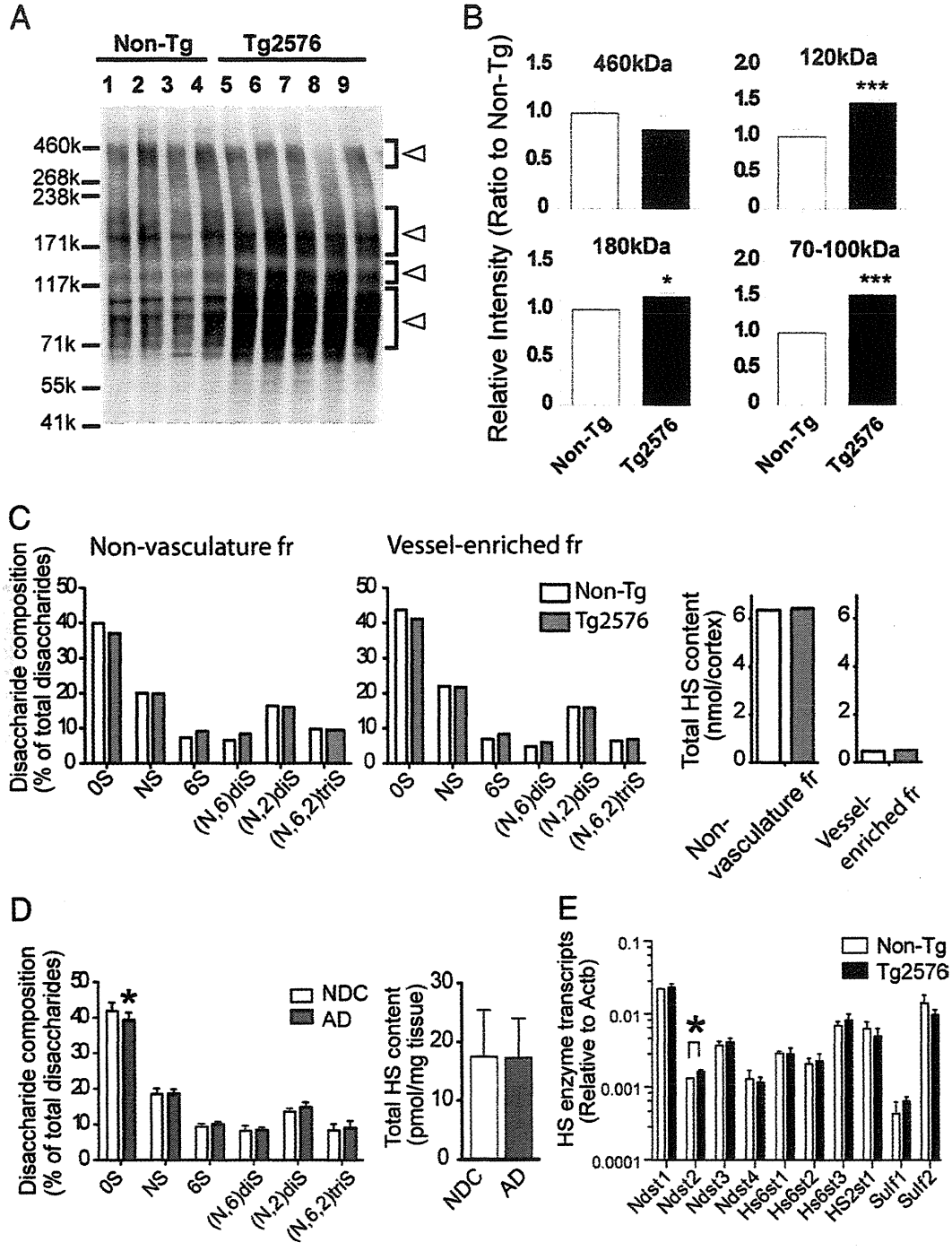


**Figure 4.** Immunoblotting analysis of the RB4CD12 epitope, disaccharide composition analysis of Heparan sulfate (HS) and quantitative real-time PCR analysis of HS enzymes in the brain of Tg2576 mice. **A:** Tris-buffered saline (TBS)-insoluble/1% SDS-soluble fractions were prepared from tissue homogenates of four 20-month-old Tg2576 (lanes 1–4) and five 20-month-old non-Tg (lanes 5–9) cortices. Immunoblot with RB4CD12 was performed as described in *Materials and Methods*. **B:** Relative intensities of bands with molecular weights of 460 kDa, 180 kDa, 120 kDa, and 70 to 100 kDa indicated by **open arrowheads** in (**A**) were measured. **C:** High performance liquid chromatography analysis determined non-sulfated (0S), monosulfated (NS, 6S), disulfated ([N,6]diS, [N,2]diS) and trisulfated ([N,6,2]triS) disaccharide compositions in non-vasculature fractions and vessel-enriched fractions of 18-month-old non-Tg and Tg2576 cortices. The level of total HS was determined by summing amounts of all disaccharides detected in each fraction. The values are representative of two independent experiments. **D:** HS disaccharide compositions and the level of total HS in the entorhinal cortex of non-demented control (NDC) ($n = 8$) and Alzheimer's disease (AD) ($n = 8$) postmortem brains were determined. **E:** Total-RNA from the cerebral cortices of 18-month-old Non-Tg ($n = 3$) and Tg2576 mice ($n = 3$) were prepared and tested. mRNA levels of 10 HS modification enzymes were determined by quantitative real-time PCR. $^{*}P < 0.05$, $^{***}P < 0.001$.

hippocampus of AD patients. Microtubule-associated protein Tau is the major protein subunit of intraneuronal neurofibrillary tangles, another neuropathological hallmark of AD.[42] It has been shown that Tau and HS coexist in nerve cells with overt neurofibrillary lesion.[33] The filamentous structures induced by heparin are structurally similar to those found in Alzheimer's disease.[43–45] We have shown that some of RB4CD12

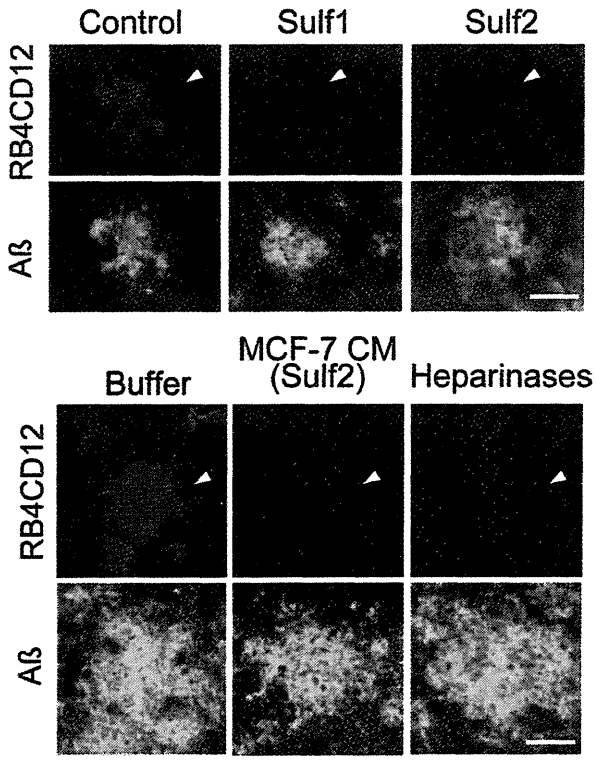


**Figure 5.** The RB4CD12 epitope in amyloid plaques of Tg2576 mouse brains is degraded *ex vivo* by Sulf-1, Sulf-2 and conditioned medium of Sulf-2-expressing cells. Cryostat-cut consecutive sections of 18-month-old Tg2576 mouse brains were incubated overnight with recombinant human Sulf-1 and Sulf-2 prepared from CM of transfected HEK293 cells (Sulf1, Sulf2), buffer only (Buffer), or CM of MCF-7 human breast cancer cells (MCF-7 CM).[8,23] The Ni-NTA resin-bound materials that were prepared from HEK293 cells transfected with the empty vector were eluted and used (control). A mix of bacterial heparinases (heparinases) served as a positive control. RB4CD12 binding was visualized using a Cy3-conjugated anti-VSV tag antibody (red). Treated sections were co-stained with 82E1 anti-Aβ antibody (green). The data are representative of two independent experiments. **Arrowheads** indicate amyloid plaques. Scale bars: 20 μm.

staining signals were found in cells that were stained with AT180, an antibody against hyperphosphorylated tau. Our results suggest that highly sulfated domains of HS might play a role in the formation of neurofibrillary tangles.

In immunoblots of brain lysates with the RB4CD12 antibody, we detected several RB4CD12-positive bands in non-Tg and Tg2576 mouse brains and found that 180 kDa, 120 kDa, and 100–70 kDa bands were upregulated in the cortex of Tg2576 mice. There were no significant changes in the intensities of 460 kDa bands. Our previous results showed that the RB4CD12 epitope is abundant in the basement membrane of the brain vessels and that the RB4CD12-positive bands were predominantly 460 kDa bands in brain vessel fractions.[9] In our immunohistochemical studies, non-vascular RB4CD12 staining was increased in Tg2576 mice. These results suggest that upregulation of 180 kDa, 120 kDa, and 100–70 kDa bands could contribute to the RB4CD12 staining colocalized with amyloid plaques in Tg2576 mouse brain. Several HSPGs are known to be localized in amyloid plaques.[14,46–49] Because of the high molecular weight (>210 kDa) of agrin and perlecan, it is conceivable that the observed signals in immunoblots might have arisen from other molecules. Syndecan-3 and glypican-1 in glial cells were identified as molecules associated with Aβ deposits.[22] Our Western blotting results suggested that syndecan-3 with the molecular weights of 180 to 250 kDa could be an HSPG that possesses the RB4CD12 epitope. However, we cannot rule out the possibility that degradation products of agrin or perlecan could harbor the RB4CD12 epitope observed in amyloid plaques. We should also pay attention to possible accumulation of HS degradation products catalyzed by nitric oxide.[50]

Unexpectedly, the trisulfated disaccharide composition was not increased in either Tg2576 or human postmortem AD brains. The mechanisms underlying the accumulation of the RB4CD12 highly sulfated domains within HS polysaccharides in non-vasculature amyloid plaques are not clear. There are two possibilities to explain the mechanisms. First, the N-sulfation of glucosamine residues is the initial HS sulfation and the N-sulfated domains are primary sites for further modification.[51] Consecutive occurrence of N-sulfation could be attributable to the formation of trisulfated disaccharide clusters, namely, highly sulfated domains, within HS chains in non-vasculature spaces. Second, translocation of HS that contains the RB4CD12 highly sulfated domains between brain vasculature and non-vasculature could be an explanation for the accumulation of the RB4CD12 epitope in Tg2576 brain parenchyma. Our findings that comparable levels of disaccharide compositions and HS contents in vessel-enriched fractions and non-vasculature fractions in the cortex of Tg2576 were shown and that the mRNA level of N-deacetylase/N-sulfotransferase 2 was increased in the cortex of Tg2576 mouse could support the former possibility. A previous study by Lindahl et al[52] showed altered distribution of N-sulfated glucosamine residues within HS extracted from postmortem AD brain. Highly N-sulfated HS may be involved in the initiation of the aggregation process of Aβ in AD brains.[53] These studies also support the former possibility as an explanation of the mechanisms of accumulation of RB4CD12-positive highly sulfated domains in Aβ plaques. We cannot rule out the possibility that the RB4CD12 epitope is a minor component and that the structural analysis we have performed might not fully detect the minor change. Quantitative analysis for the RB4CD12-positive HS in the cortex would make advances in the study of the mechanisms.

Herein, we found that the RB4CD12 epitope accumulated in amyloid plaques can be degraded by Sulf-1 and Sulf-2 *ex vivo*. It was suggested that the RB4CD12 highly sulfated domains are localized at the surface of amyloid plaques, as these HS degrading enzymes could access and efficiently degrade the epitope. Although the RB4CD12 epitope in amyloid plaques was degraded by the Sulfs, substantial amounts of Aβ were retained in these plaques. This result suggests that the highly sulfated domains of HS universally associated with amyloid deposits in the brain. Accumulation of the RB4CD12 epitope in amyloid plaques could induce excessive entrapment of growth factors at amyloid plaques, which might lead to an imbalance in homeostasis of the brain microenvironment. Increasing evidence points to vascular damage as an early contributor in Alzheimer pathology.[54,55] A recent study suggested that angiogenesis

might be impaired in AD model mice,[56] despite the fact that the levels of pro-angiogenic growth factors (eg, vascular endothelial growth factor [VEGF]) are elevated in AD brains.[57–59] VEGF binds to immobilized heparin and can be stored in the extracellular space by binding to HS and HSPG.[23,60] Heparin-bound VEGF is mobilized by the action of Sulf-2, which exerts pro-angiogenic activity.[23,61] VEGF is found to be associated with amyloid plaques in AD, but not non-AD brain.[62] Our results also suggested that the highly sulfated domains could be involved in sequestration of VEGF within amyloid plaques and vascular damage in AD through perturbation in the supply of pro-angiogenic growth factors. Aberrant angiogenesis could induce neurovascular uncoupling, which ultimately leads to synaptic dysfunction.[63] In summary, we provide evidence that highly sulfated domains recognized by RB4CD12 accumulated in amyloid plaques of brains of AD model mice and patients with AD. Further studies to investigate the roles of the highly sulfated HS domains with special regard to angiogenesis in AD pathology will be needed.

## *Acknowledgments*

We thank Steven Rosen and Yoshiko Takeda-Uchimura for their helpful suggestions and discussions. We also thank Kuniko Takanose, Noriko Sugaya, and Hudson Johns for their technical assistance. We are grateful to Yoshio Hashizume and Takayuki Yamamoto for their diagnostic examination and support.

## *References*

1. Bernfield M, Gotte M, Park PW, Reizes O, Fitzgerald ML, Lincecum J, Zako M: Functions of cell surface heparan sulfate proteoglycans. Annu Rev Biochem 1999, 68:729–777
2. Esko JD, Lindahl U: Molecular diversity of heparan sulfate. J Clin Invest 2001, 108:169–173
3. Gallagher JT: Heparan sulfate: growth control with a restricted sequence menu. J Clin Invest 2001, 108:357–361
4. Nakato H, Kimata K: Heparan sulfate fine structure and specificity of proteoglycan functions. Biochim Biophys Acta 2002, 1573:312–318
5. Parish CR: The role of heparan sulphate in inflammation. Nat Rev Immunol 2006, 6:633–643
6. Bishop JR, Schuksz M, Esko JD: Heparan sulphate proteoglycans fine-tune mammalian physiology. Nature 2007, 446:1030–1037
7. Dennissen MA, Jenniskens GJ, Pieffers M, Versteeg EM, Petitou M, Veerkamp JH, van Kuppevelt TH: Large, tissue-regulated domain diversity of heparan sulfates demonstrated by phage display antibodies. J Biol Chem 2002, 277:10982–10986
8. Hossain MM, Hosono-Fukao T, Tang R, Sugaya N, van Kuppevelt TH, Jenniskens GJ, Kimata K, Rosen SD, Uchimura K: Direct detection of HSulf-1 and HSulf-2 activities on extracellular heparan sulfate and their inhibition by PI-88. Glycobiology 2010, 20:175–186
9. Hosono-Fukao T, Ohtake-Niimi S, Nishitsuji K, Hossain MM, van Kuppevelt TH, Michikawa M, Uchimura K: RB4CD12 epitope expression and heparan sulfate disaccharide composition in brain vasculature. J Neurosci Res 2011, 89:1840–1848
10. Esko JD, Selleck SB: Order out of chaos: assembly of ligand binding sites in heparan sulfate. Annu Rev Biochem 2002, 71:435–471
11. Saad OM, Ebel H, Uchimura K, Rosen SD, Bertozzi CR, Leary JA: Compositional profiling of heparin/heparan sulfate using mass spectrometry: assay for specificity of a novel extracellular human endosulfatase. Glycobiology 2005, 15:818–826
12. Morimoto-Tomita M, Uchimura K, Werb Z, Hemmerich S, Rosen SD: Cloning and characterization of two extracellular heparin-degrading endosulfatases in mice and humans. J Biol Chem 2002, 277:49175–49185
13. Snow AD, Mar H, Nochlin D, Kimata K, Kato M, Suzuki S, Hassell J, Wight TN: The presence of heparan sulfate proteoglycans in the neuritic plaques and congophilic angiopathy in Alzheimer's disease. Am J Pathol 1988, 133:456–463
14. Snow AD, Sekiguchi RT, Nochlin D, Kalaria RN, Kimata K: Heparan sulfate proteoglycan in diffuse plaques of hippocampus but not of cerebellum in Alzheimer's disease brain. Am J Pathol 1994, 144: 337–347
15. Snow AD, Sekiguchi R, Nochlin D, Fraser P, Kimata K, Mizutani A, Arai M, Schreier WA, Morgan DG: An important role of heparan sulfate proteoglycan (Perlecan) in a model system for the deposition and persistence of fibrillar A beta-amyloid in rat brain. Neuron 1994, 12:219–234
16. van Horssen J, Wesseling P, van den Heuvel LP, de Waal RM, Verbeek MM: Heparan sulphate proteoglycans in Alzheimer's disease and amyloid-related disorders. Lancet Neurol 2003, 2:482–492
17. Watson DJ, Lander AD, Selkoe DJ: Heparin-binding properties of the amyloidogenic peptides Abeta and amylin. Dependence on aggregation state and inhibition by Congo red. J Biol Chem 1997, 272: 31617–31624
18. Hsiao K, Chapman P, Nilsen S, Eckman C, Harigaya Y, Younkin S, Yang F, Cole G: Correlative memory deficits. A beta elevation, and amyloid plaques in transgenic mice, Science 1996, 274:99–102
19. Mucke L, Masliah E, Yu GQ, Mallory M, Rockenstein EM, Tatsuno G, Hu K, Kholodenko D, Johnson-Wood K, McConlogue L: High-level neuronal expression of abeta 1–42 in wild-type human amyloid protein precursor transgenic mice: synaptotoxicity without plaque formation. J Neurosci 2000, 20:4050–4058
20. Rockenstein E, Mallory M, Mante M, Sisk A, Masliaha E: Early formation of mature amyloid-beta protein deposits in a mutant APP transgenic model depends on levels of A beta(1–42). J Neurosci Res 2001, 66:573–582
21. Jenniskens GJ, Oosterhof A, Brandwijk R, Veerkamp JH, van Kuppevelt TH: Heparan sulfate heterogeneity in skeletal muscle basal lamina: demonstration by phage display-derived antibodies. J Neurosci 2000, 20:4099–4111
22. O'Callaghan P, Sandwall E, Li JP, Yu H, Ravid R, Guan ZZ, van Kuppevelt TH, Nilsson LN, Ingelsson M, Hyman BT, Kalimo H, Lindahl U, Lannfelt L, Zhang X: Heparan sulfate accumulation with Abeta deposits in Alzheimer's disease and Tg2576 mice is contributed by glial cells. Brain Pathol 2008, 18:548–561
23. Uchimura K, Morimoto-Tomita M, Bistrup A, Li J, Lyon M, Gallagher J, Werb Z, Rosen SD: HSulf-2, an extracellular endoglucosamine-6-sulfatase, selectively mobilizes heparin-bound growth factors and chemokines: effects on VEGF. FGF-1, and SDF-1, BMC Biochem 2006, 7:2
24. Christie R, Yamada M, Moskowitz M, Hyman B: Structural and functional disruption of vascular smooth muscle cells in a transgenic mouse model of amyloid angiopathy. Am J Pathol 2001, 158:1065–1071
25. Diaz-Nido J, Wandosell F, Avila J: Glycosaminoglycans and beta-amyloid, prion and tau peptides in neurodegenerative diseases. Peptides 2002, 23:1323–1332
26. McLaurin J, Fraser PE: Effect of amino-acid substitutions on Alzheimer's amyloid-beta peptide-glycosaminoglycan interactions. Eur J Biochem 2000, 267:6353–6361
27. Gupta-Bansal R, Frederickson RC, Brunden KR: Proteoglycan-mediated inhibition of A beta proteolysis. A potential cause of senile plaque accumulation, J Biol Chem 1995, 270:18666–18671
28. Ancsin JB, Kisilevsky R: The heparin/heparan sulfate-binding site on apo-serum amyloid A. Implications for the therapeutic intervention of amyloidosis, J Biol Chem 1999, 274:7172–7181
29. Cohlberg JA, Li J, Uversky VN, Fink AL: Heparin and other glycosaminoglycans stimulate the formation of amyloid fibrils from alpha-synuclein in vitro. Biochemistry 2002, 41:1502–1511
30. Supattapone S: Prion protein conversion in vitro. J Mol Med 2004, 82:348–356
31. Motamedi-Shad N, Monsellier E, Torrassa S, Relini A, Chiti F: Kinetic analysis of amyloid formation in the presence of heparan sulfate: faster unfolding and change of pathway. J Biol Chem 2009, 284: 29921–29934

32. Noborn F, O'Callaghan P, Hermansson E, Zhang X, Ancsin JB, Damas AM, Macklin I, Presto J, Johansson J, Saraiva MJ, Lundgren E, Kisilevsky R, Westermark P, Li JP: Heparan sulfate/heparin promotes transthyretin fibrillization through selective binding to a basic motif in the protein. Proc Natl Acad Sci USA 2011, 108:5584–5589
33. Goedert M, Jakes R, Spillantini MG, Hasegawa M, Smith MJ, Crowther RA: Assembly of microtubule-associated protein tau into Alzheimer-like filaments induced by sulphated glycosaminoglycans. Nature 1996, 383:550–553
34. McLaurin J, Franklin T, Zhang X, Deng J, Fraser PE: Interactions of Alzheimer amyloid-beta peptides with glycosaminoglycans effects on fibril nucleation and growth. Eur J Biochem 1999, 266:1101–1110
35. Castillo GM, Lukito W, Wight TN, Snow AD: The sulfate moieties of glycosaminoglycans are critical for the enhancement of beta-amyloid protein fibril formation. J Neurochem 1999, 72:1681–1687
36. Valle-Delgado JJ, Alfonso-Prieto M, de Groot NS, Ventura S, Samitier J, Rovira C, Fernandez-Busquets X: Modulation of Abeta42 fibrillogenesis by glycosaminoglycan structure. FASEB J 2010, 24:4250–4261
37. Li JP, Galvis ML, Gong F, Zhang X, Zcharia E, Metzger S, Vlodavsky I, Kisilevsky R, Lindahl U: In vivo fragmentation of heparan sulfate by heparanase overexpression renders mice resistant to amyloid protein A amyloidosis. Proc Natl Acad Sci USA 2005, 102:6473–6477
38. Timmer NM, Schirris TJ, Bruinsma IB, Otte-Holler I, van Kuppevelt TH, de Waal RM, Verbeek MM: Aggregation and cytotoxic properties towards cultured cerebrovascular cells of Dutch-mutated Abeta40 (DAbeta(1–40)) are modulated by sulfate moieties of heparin. Neurosci Res 2010, 66:380–389
39. Meyer-Luehmann M, Coomaraswamy J, Bolmont T, Kaeser S, Schaefer C, Kilger E, Neuenschwander A, Abramowski D, Frey P, Jaton AL, Vigouret JM, Paganetti P, Walsh DM, Mathews PM, Ghiso J, Staufenbiel M, Walker LC, Jucker M: Exogenous induction of cerebral beta-amyloidogenesis is governed by agent and host. Science 2006, 313:1781–1784
40. Timmer NM, Herbert MK, Kleinovink JW, Kiliaan AJ, De Waal RM, Verbeek MM: Limited expression of heparan sulphate proteoglycans associated with Abeta deposits in the APPswe/PS1dE9 mouse model for Alzheimer's disease. Neuropathol Appl Neurobiol 2010, 36:478–486
41. van den Born J, Salmivirta K, Henttinen T, Ostman N, Ishimaru T, Miyaura S, Yoshida K, Salmivirta M: Novel heparan sulfate structures revealed by monoclonal antibodies. J Biol Chem 2005, 280:20516–20523
42. Skovronsky DM, Lee VM, Trojanowski JQ: Neurodegenerative diseases: new concepts of pathogenesis and their therapeutic implications. Annu Rev Pathol 2006, 1:151–170
43. Kuret J, Chirita CN, Congdon EE, Kannanayakal T, Li G, Necula M, Yin H, Zhong Q: Pathways of tau fibrillization. Biochim Biophys Acta 2005, 1739:167–178
44. Perez M, Valpuesta JM, Medina M, Montejo de Garcini E, Avila J: Polymerization of tau into filaments in the presence of heparin: the minimal sequence required for tau-tau interaction. J Neurochem 1996, 67:1183–1190
45. Zhu HL, Fernandez C, Fan JB, Shewmaker F, Chen J, Minton AP, Liang Y: Quantitative characterization of heparin binding to Tau protein: implication for inducer-mediated Tau filament formation. J Biol Chem 2010, 285:3592–3599
46. Van Gool D, David G, Lammens M, Baro F, Dom R: Heparan sulfate expression patterns in the amyloid deposits of patients with Alzheimer's and Lewy body type dementia. Dementia 1993, 4:308–314
47. Donahue JE, Berzin TM, Rafii MS, Glass DJ, Yancopoulos GD, Fallon JR, Stopa EG: Agrin in Alzheimer's disease: altered solubility and abnormal distribution within microvasculature and brain parenchyma, Proc Natl Acad Sci USA 1999, 96:6468–6472
48. Verbeek MM, Otte-Holler I, van den Born J, van den Heuvel LP, David G, Wesseling P, de Waal RM: Agrin is a major heparan sulfate proteoglycan accumulating in Alzheimer's disease brain. Am J Pathol 1999, 155:2115–2125
49. van Horssen J, Otte-Holler I, David G, Maat-Schieman ML, van den Heuvel LP, Wesseling P, de Waal RM, Verbeek MM: Heparan sulfate proteoglycan expression in cerebrovascular amyloid beta deposits in Alzheimer's disease and hereditary cerebral hemorrhage with amyloidosis (Dutch) brains. Acta Neuropathol 2001, 102:604–614
50. Cappai R, Cheng F, Ciccotosto GD, Needham BE, Masters CL, Multhaup G, Fransson LA, Mani K: The amyloid precursor protein (APP) of Alzheimer disease and its paralog. APLP2, modulate the Cu/Zn-Nitric Oxide-catalyzed degradation of glypican-1 heparan sulfate in vivo, J Biol Chem 2005, 280:13913–13920
51. Carlsson P, Presto J, Spillmann D, Lindahl U, Kjellen L: Heparin/heparan sulfate biosynthesis: processive formation of N-sulfated domains. J Biol Chem 2008, 283:20008–20014
52. Lindahl B, Eriksson L, Lindahl U: Structure of heparan sulphate from human brain, with special regard to Alzheimer's disease, Biochem J 1995, 306 (Pt 1):177–184
53. Bruinsma IB, te Riet L, Gevers T, ten Dam GB, van Kuppevelt TH, David G, Kusters B, de Waal RM, Verbeek MM: Sulfation of heparan sulfate associated with amyloid-beta plaques in patients with Alzheimer's disease. Acta Neuropathol 2010, 119:211–220
54. Bailey TL, Rivara CB, Rocher AB, Hof PR: The nature and effects of cortical microvascular pathology in aging and Alzheimer's disease. Neurol Res 2004, 26:573–578
55. Meyer EP, Ulmann-Schuler A, Staufenbiel M, Krucker T: Altered morphology and 3D architecture of brain vasculature in a mouse model for Alzheimer's disease, Proc Natl Acad Sci USA 2008, 105:3587–3592
56. Paris D, Ganey N, Banasiak M, Laporte V, Patel N, Mullan M, Murphy SF, Yee GT, Bachmeier C, Ganey C, Beaulieu-Abdelahad D, Mathura VS, Brem S: Impaired orthotopic glioma growth and vascularization in transgenic mouse models of Alzheimer's disease. J Neurosci 2010, 30:11251–11258
57. Kalaria RN, Cohen DL, Premkumar DR, Nag S, LaManna JC, Lust WD: Vascular endothelial growth factor in Alzheimer's disease and experimental cerebral ischemia. Brain Res Mol Brain Res 1998, 62: 101–105
58. Tarkowski E, Issa R, Sjogren M, Wallin A, Blennow K, Tarkowski A, Kumar P: Increased intrathecal levels of the angiogenic factors VEGF and TGF-beta in Alzheimer's disease and vascular dementia. Neurobiol Aging 2002, 23:237–243
59. Siedlak SL, Cras P, Kawai M, Richey P, Perry G: Basic fibroblast growth factor binding is a marker for extracellular neurofibrillary tangles in Alzheimer disease. J Histochem Cytochem 1991, 39:899–904
60. Iozzo RV: Matrix proteoglycans: from molecular design to cellular function. Annu Rev Biochem 1998, 67:609–652
61. Morimoto-Tomita M, Uchimura K, Bistrup A, Lum DH, Egeblad M, Boudreau N, Werb Z, Rosen SD: Sulf-2, a proangiogenic heparan sulfate endosulfatase, is upregulated in breast cancer. Neoplasia 2005, 7:1001–1010
62. Ryu JK, Cho T, Choi HB, Wang YT, McLarnon JG: Microglial VEGF receptor response is an integral chemotactic component in Alzheimer's disease pathology. J Neurosci 2009, 29:3–13
63. Zlokovic BV: Neurovascular mechanisms of Alzheimer's neurodegeneration. Trends Neurosci 2005, 28:202–208

BRAIN RESEARCH ▮ (▮▮▮▮) ▮▮▮–▮▮▮

Available online at www.sciencedirect.com

SciVerse ScienceDirect

www.elsevier.com/locate/brainres

Brain Research

Research Report

# Enhancement of FGF-1 release along with cytosolic proteins from rat astrocytes by hydrogen peroxide

*Jin-ichi Ito*[a,*], *Yuko Nagayasu*[a], *Mariko Hoshikawa*[a], *Koichi H. kato*[b], *Yutaka Miura*[c], *Kiyofumi Asai*[c], *Hideki Hayashi*[d], *Shinji Yokoyama*[a,e], *Makoto Michikawa*[a]

[a]*Biochemistry and Molecular Neurobiology, Nagoya City University Graduate School of Medical Sciences, Nagoya 467-8601, Japan*

[b]*Graduate School of Natural Sciences, Nagoya City University, Nagoya 467-8501, Japan*

[c]*Bioregulation and Molecular Neurobiology, Nagoya City University Graduate School of Medical Sciences, Nagoya 467-8601, Japan*

[d]*Priority Organization for Innovation and Excellence, Kumamoto University, 1-1-1 Honjo, Kumamoto 860-8556, Japan*

[e]*Food and Nutritional Sciences, College of Bioscience and Biotechnology, Chubu University, Matsumoto-cho 1200, Kasugai 487-8501, Japan*

ARTICLE INFO

*Article history:*
Accepted 22 May 2013

*Keywords:*
Oxidative stress
Astrocytes
FGF-1 release
Long-term culture

ABSTRACT

We previously observed that the production and release of fibroblast growth factor (FGF-1) are increased in rat astrocytes during in vitro long-term culture, that FGF-1 enhances the generation of apoE-containing high density lipoproteins (apoE/HDL), and that the wound healing of brain cryoinjury delays in apoE-deficient mouse. The detail mechanism underlying these phenomena remains unknown. In this study, we examined effects of oxidative stress on release of FGF-1 from cultured rat astrocytes.

The treatment of rat astrocytes with 100 μM hydrogen peroxide ($H_2O_2$) for 10 min enhanced FGF-1 release without inducing apoptosis. The conditioned medium prepared from the cells cultured in a fresh medium after the treatment with $H_2O_2$ had the FGF-1-like activities, which enhanced cholesterol synthesis, signalings to phosphorylate Akt and ERK, and apoE secretion. The oxidative stress induced by $H_2O_2$ enhanced the release of cytosolic proteins such as HSP70 and HSP90 in addition to FGF-1. Antioxidants such as ascorbic acid and ebselen suppressed the release of cytosolic proteins induced by $H_2O_2$ treatment. The addition of lipoproteins such as low density lipoproteins (LDL), furthermore, canceled $H_2O_2$-induced release of FGF-1 and cytosolic proteins. Proteolysis of cytosolic proteins in the $H_2O_2$-treated rat astrocytes was enhanced in the presence of exogenous trypsin, which was attenuated by the pretreatment with LDL, suggesting that $H_2O_2$ increases the permeability of

Abbreviations: BBB, blood brain barrier; apo, apolipoprotein; DPBS, Dulbecco's phosphate-buffered saline; BSA, bovine serum albumin; CNS, central nervous system; CSF, cerebrospinal fluid; DMEM, Dulbecco's modified Eagle's medium; FGF-1, fibroblast growth factor 1; FCS, fetal calf serum; HDL, high density lipoproteins; LDH, lactate dehydrogenase; TLC, thin layer chromatography; SDS-PAGE, 0.5% SDS/12.5% polyacrylamide gel electrophoresis; TCA, trichloroacetic acid; RT-PCR, reverse transcription-polymerase chain reaction

*Correspondence to: Department of Biochemistry, Nagoya City University Graduate School of Medical Sciences, Kawasumi 1, Mizuho-cho, Mizuho-ku, Nagoya 467-8601, Japan. Fax: +81 52 841 3480.
*E-mail address:* jitoh@med.nagoya-cu.ac.jp (J.-i. Ito).

0006-8993/$ - see front matter 
http://dx.doi.org/10.1016/j.brainres.2013.05.035

the membrane of cells, which was prevented by the addition of lipoproteins. These findings suggest that oxidative stress is one of the candidates which triggers FGF-1 release from astrocytes in the brain, and that the lipid homeostasis in the cell membrane may regulate $H_2O_2$-induced release of FGF-1.



## 1. Introduction

ApoE is the most abundant apolipoprotein and plays an important role in intercellular transport of cholesterol forming apoE/HDL in the brain, where the cholesterol supply is segregated by the blood–brain barrier (BBB) from the lipoprotein system in the circulation (Dietschy and Turley, 2001; Linton et al., 1991). Astrocytes synthesize apoE and cholesterol and release them as apoE/HDL for intercellular cholesterol delivery in CNS (Ito et al., 1999). HDL may play an important role in cholesterol homeostasis in CNS (Ito and Yokoyama, 2004). We found that fibroblast growth factor 1 (FGF-1, acidic FGF) enhances apoE/HDL generation of astrocytes accompanied by the up-regulation of syntheses of apoE and cholesterol, very likely in an autocrine manner (Ito et al., 2005, 2007; Lu et al., 2009; Nagayasu et al., 2008). It was also shown by immunohistochemical analysis that the productions of FGF-1 and apoE are increased in the astrocytes around a cryoinjury-induced lesion in the mouse brain. Wound healing is substantially delayed in apoE-deficient mice, although the production of FGF-1 is increased in the injured brain also (Tada et al., 2004). The production and release of FGF-1 are enhanced in rat astrocytes under the long-term cultured stress (Ito et al., 2005; Ueno et al., 2002). These findings suggest that injury and stress induce astrocytes to produce and secrete FGF-1 and up-regulate apoE/HDL generation to promote wound healing as well. However, the mechanism underlying cryoinjury-induced increase in the expression levels of FGF-1 and apoE remains unknown.

FGF-1 belongs to the FGF family and stimulates the proliferation and differentiation of mesodermal and neuroectodermal cells such as fibroblasts and astrocytes, similarly to FGF-2 (basic FGF) (Larsson et al., 1999; Dono, 2003). FGF-1 is known to localize in all motor neurons and primary sensory neurons in the mesencephalon and in a small number of glial cells in the white matter (Eckenstein et al., 1994; Eckenstein, 1994). In Alzheimer's disease, some astrocytes are reportedly stained for FGF-1 in both the gray and white matters (Tooyama et al., 1991). FGF-1 has been shown to contribute to neuron survival, neurite outgrowth, and angiogenesis in vitro and in vivo (Tada et al., 2004; Mohiuddin et al., 1996).

Because FGF-1 and FGF-2 have no amino-terminal signal sequence, these factors are considered to be synthesized and to localize in the cytosol and nucleus of FGF-producing cells (Mason, 1994; Wiedlocha et al., 2005). Accordingly, their release to the extracellular space is unlikely mediated by the classical intracellular transport system through the endoplasmic reticulum (ER)/Golgi pathway after their biosynthesis. The mechanism of FGF-1 release is unclear at present despite of some previous investigation (Carreira et al., 1998; Prudovsky et al., 2003; Mohan et al., 2010). Consistent with our findings (Ito et al., 2005; Ueno et al., 2002), FGF-1 seems to be released in response to sublethal cell injuries such as oxidative stress, heat shock, hypoxia, and serum starvation (Jackson et al., 1992; Shin et al., 1996; Opalenic et al., 1998; Mouta et al., 2001). Previous reports have shown that FGF-1 is expressed in reactive astrocytes in the brains of patients with Alzheimer's disease (Mashayekhi et al., 2010), which is known to be associated with chronic inflammation and oxidative stress (Pratico and Trojanowski, 2000; Pratico and Delanty, 2000). These lines of evidence suggest that FGF-1 release is enhanced under oxidative stress conditions, which can in turn stimulates apoE/HDL generation in the brain. It is, thus, possible that astrocytes protect neurons from stress and injury through the FGF-1/apoE/HDL system. Therefore, it is important to observe that astrocytes practically release FGF-1 under oxidative stress in the process of studies to prove that astrocytes release FGF-1 to upregulate apoE/HDL generation of astrocytes in the manner of autocrine action for brain protection against various stresses. In the present study, we especially examined in vitro whether the release of FGF-1 from the brain-derived astrocytes is actually triggered by oxidative stress.

## 2. Results

In order to examine FGF-1 release under oxidative stress induced by $H_2O_2$, we attempted to determine the experimental conditions that induce oxidative stress without inducing apoptosis in rat astrocytes conventionally cultured for one week. Paster et al. (2009) have already reported that the viability of mouse astrocytes remains approximately 100% after treatment with 100 μM $H_2O_2$ for 24 h. We also observed that the apoptosis is not apparently induced in rat astrocytes treated with 100 μM $H_2O_2$ within 18 h after the commencement of $H_2O_2$ addition, as shown in Fig. 1A. The cellular level of lactate dehydrogenase (LDH) in cultured rat astrocytes did not significantly decrease in the cells treated with $H_2O_2$ at 1 h, but decreased by 12.5% or 20.4% at 4 h after the commencement of the treatment with 100 or 300 μM $H_2O_2$, respectively (Fig. 1B). These findings suggest that the treatment with 100 μM $H_2O_2$ for 1 h hardly induces apoptosis in rat astrocytes. On the basis of these findings, the treatment of the cells with 100 μM $H_2O_2$ for 10 min was employed in the following experiments to examine FGF-1 release without inducing apoptosis. Although the treatment with 100 μM $H_2O_2$ for 10 min inhibited transiently syntheses of cholesterol and sphingomyelin in rat astrocytes, these syntheses were restored approximately 24 h after withdraw of $H_2O_2$ (Fig. 1C).

We examined whether the FGF-1-like factor, which enhances apoE secretion, signalings to phosphorylate Akt, MEK, and ERK, and cholesterol synthesis, is released from

Please cite this article as: Ito, J., et al., Enhancement of FGF-1 release along with cytosolic proteins from rat astrocytes by hydrogen peroxide, (2013), http://dx.doi.org/10.1016/j.brainres.2013.05.035

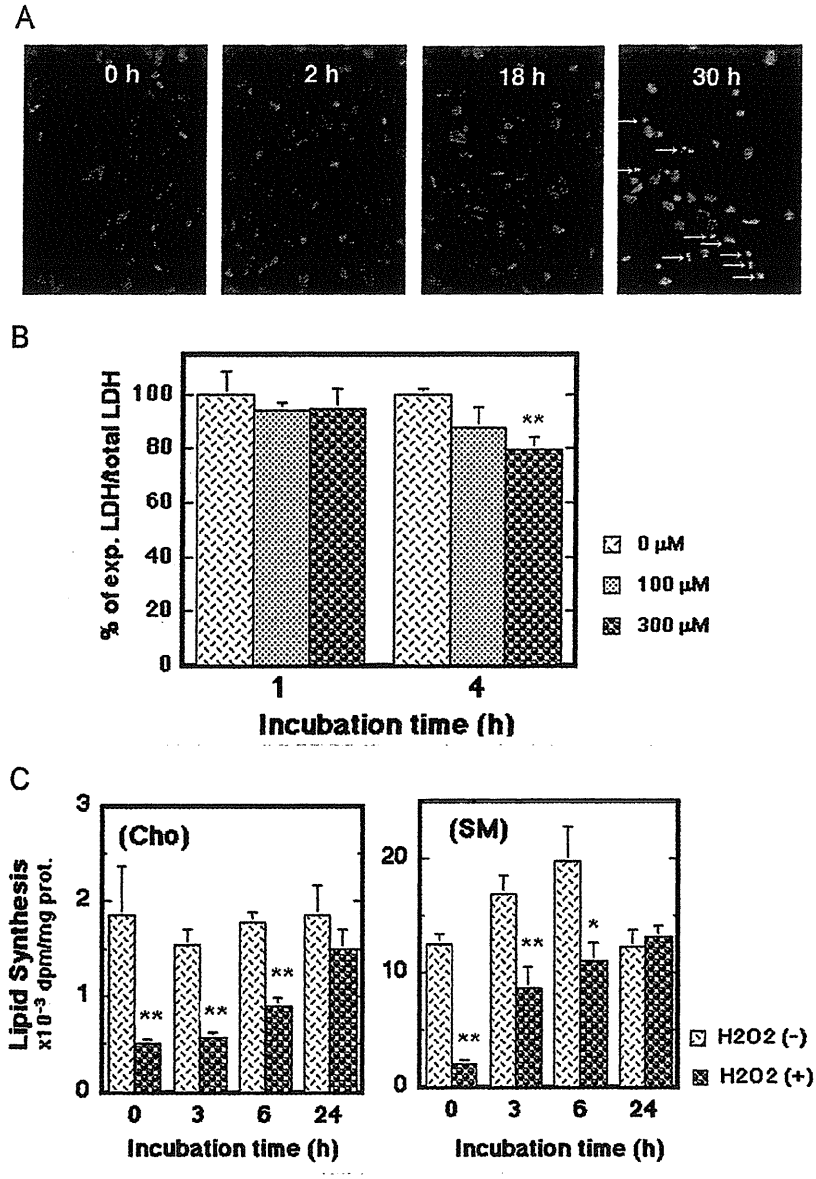


**Fig. 1 – Cytotoxicity of hydrogen peroxide to rat astrocytes. Apoptosis of rat astrocytes treated with 100 μM $H_2O_2$ for 0, 2, 18, or 30 h was observed by using Vybrant™ Apoptosis Assay Kit #5. Arrows indicate the changes in staining that are significant (A). Rat astrocytes were treated with $H_2O_2$ (0, 100, or 300 μM) in 0.1% BSA/F-10 for 1 or 4 h. Cellular LDH label in the cytosol fraction prepared in accordance with the method described in Experimental Procedure was determined using a CytoTox 96 Non-Radioactive Cytotoxicity Assay kit (promega). The cytotoxicity of $H_2O_2$ was examined to determine the percentage of cytosolic LDH level in rat astrocytes treated with $H_2O_2$ with respect to that in control cells treated without $H_2O_2$. Results are shown as means±SD, **$P<0.01$, significantly different from the value obtained from the cells treated without $H_2O_2$ (B). After washing 3 times with DPBS and replacement with 0.1% BSA/F-10, rat astrocytes were treated with or without 100 μM $H_2O_2$ for 10 min and washed 4 times. The cells were incubated in 0.02% BSA/F-10 for 0, 3, 6, or 24 h and then incubated with [$^{14}$C]-acetate (2 μCi/ml) in a fresh 0.02% BSA/F-10 for 2 h. The lipid was extracted from the cells and analyzed by thin layer chromatography (TLC) according to the method in Experimental Procedure for cholesterol (Cho) or sphingomyelin (SM). The data points represent the means±SD, **, $P<0.01$, significantly different from the value of cells treated without $H_2O_2$ (C).**

treated astrocytes. The conditioned medium harvested from the cultures without $H_2O_2$ treatment suppressed cholesterol biosynthesis. This may suggest that the conditioned medium contains cholesterol-rich HDL or some inhibitors to suppress cholesterol synthesis (Fig. 2A). The conditioned medium of astrocytes treated with $H_2O_2$, however, enhanced cholesterol synthesis (Fig. 2A), signalings such as the phosphorylation of Akt and ERK (Fig. 2B), and apoE secretion (Fig. 2C) in astrocytes compared with the one from the cultures without $H_2O_2$ treatment. This suggests that FGF-1-like activities exsist in the conditioned medium of astrocytes treated with $H_2O_2$. Then we examined whether $H_2O_2$ treatment enhances

Please cite this article as: Ito, J., et al., Enhancement of FGF-1 release along with cytosolic proteins from rat astrocytes by hydrogen peroxide, (2013), http://dx.doi.org/10.1016/j.brainres.2013.05.035

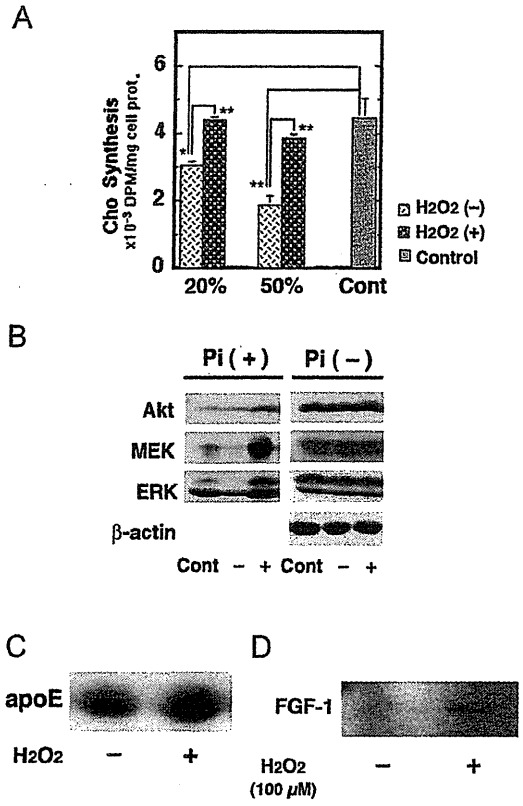


**Fig. 2 – FGF-1 release from rat astrocytes treated with $H_2O_2$. After the treatment of rat astrocytes with (+) or without (–) 100 μM $H_2O_2$ for 10 min, the conditioned medium was collected from the cells incubated in a fresh 0.02% BSA/F-10 for 24 h. Other rat astrocytes were incubated with the conditioned medium (0, 200, or 500 μl/ml; Cont, 20%, or 50%) in a fresh 0.02% BSA/F-10 for 5 h and washed with DPBS, followed by incubation with [$^{14}$C]-acetate (2 μCi/ml) for 2 h. After washing, lipids were extracted from the cells and analyzed by TLC for cholesterol. The data points represent the means±SD, **, $P<0.01$, significantly different from the value obtained using conditioned medium of cells treated without $H_2O_2$ (A). Rat astrocytes were treated with (+) or without (–) 100 μM $H_2O_2$ for 10 min and washed 4 times with DPBS, followed by incubation in a fresh 0.02% BSA/F-10 for 24 h for the preparation of conditioned media. Other rat astrocytes were incubated with or without (Cont) each conditioned medium in a fresh 0.02% BSA/F-10 (200 μl/ml) for 5 min or 16 h. The 5-min-incubated cells (100 μg of proteins) were analyzed by SDS-PAGE and Western blotting to detect Akt, MEK, ERK and β-actin (Pi (–)) and phosphorylated Akt, MEK, and ERK (Pi (+)) (B). The 16-h-incubated cells (100 μg of proteins) were washed and incubated in a fresh 0.02% BSA/F-10 for 24 h again to prepare conditioned medium. The conditioned medium was treated with 10% TCA. Proteins in the pellets were analyzed by SDS-PAGE and Western blotting using goat anti-apoE antibody (C). Rat astrocytes (2300 μg of proteins) were treated with or without 100 μM $H_2O_2$ for 10 min, washed and incubated in a fresh 0.02% BSA/F-10 for 24 h again. Heparin-sepharose was incubated with each conditioned medium at 4 °C for 16 h, washed and analyzed by SDS-PAGE and Western blotting using goat anti-FGF-1 antibody (D).**

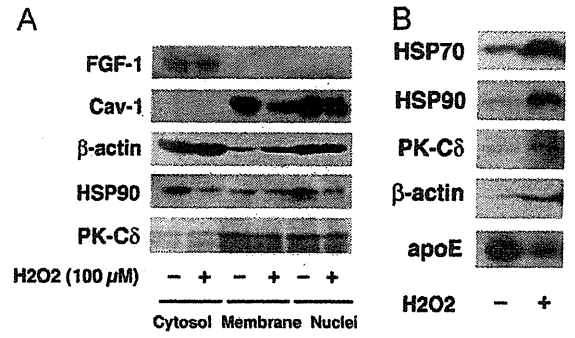


**Fig. 3 – Distribution change of cellular proteins in $H_2O_2$-treated rat astrocytes. Rat astrocytes were treated with or without 100 μM $H_2O_2$ for 10 min, washed and incubated in a fresh 0.02% BSA/F-10 for 24 h again. The cytosol (80 μg of proteins), membrane (80 μg of proteins), and nuclei fractions (80 μg of proteins) (A), or the conditioned medium (B) from the cells (100 μg of proteins) were prepared in accordance with the method described in Section 4 and analyzed by SDS-PAGE and Western blotting to detect FGF-1, caveolin-1 (Cav-1), β-actin, HSP90, HSP70, protein kinase Cδ (PK-Cδ), or apoE.**

FGF-1 release. The release of FGF-1 from $H_2O_2$-treated astrocytes was actually observed by SDS-PAGE and Western blotting analysis (Fig. 2D).

We examined the changes in intracellular levels of FGF-1 and cytosolic proteins accompanied by the FGF-1 release from $H_2O_2$-treated astrocyte. The cytosolic level of HSP90 greatly decreased as compared with intracellular FGF-1 (Fig. 3A). The β-actin level was significantly enhanced in the membrane fraction by $H_2O_2$ treatment. The levels of HSP90 and protein kinase Cδ (PK-Cδ) in the membrane fraction remained unchanged between before and after the $H_2O_2$ treatment. The export of cytosolic proteins such as HSP90, HSP70, PK-Cδ, and β-actin to the conditioned medium was enhanced in astrocytes treated with $H_2O_2$, despite of suppression of apoE secretion (Fig. 3B). This finding shows that oxidative stress enhances the release of not only FGF-1 but also cytosolic proteins and suppresses the classical intracellular transport of apoE through the ER/Golgi pathway. Molecular weight ranges of proteins released from rat astrocytes treated with or without $H_2O_2$ was showed by SDS-PAGE and autoradiography of the proteins released as [$^{35}$S]-labeled cellular proteins. The enhanced release of [$^{35}$S]-labeled cellular proteins of high molecular weights over 175 kDa was observed in the cells treated with 100 μM $H_2O_2$ (Fig. 4A). This finding suggests that the release of FGF-1 is enhanced in the FGF-1-nonspecific manner. The cytosolic protein release from the cells was also enhanced by other oxidants such as t-butyl hydroperoxide (tBHP) (Fig. 4B). Antioxidants such as ebselen and ascorbic acid suppressed the release of cytosolic proteins from the cells (Fig. 4C). Superoxide dismutase-like compound such as MnTMPyP, however, failed to suppress the release of cytosolic proteins, suggesting that superoxide does not participate in this phenomenon. Heat shock at 42 °C had no effect on enhancing the release of cytosolic proteins from the cells (Fig. 4D).

Please cite this article as: Ito, J., et al., Enhancement of FGF-1 release along with cytosolic proteins from rat astrocytes by hydrogen peroxide, (2013), http://dx.doi.org/10.1016/j.brainres.2013.05.035